Catalysis Today 140 (2009) 135–141

Contents lists available at ScienceDirect

Catalysis Today

journal homepage: www.elsevier.com/locate/cattod

Effect of promotion with ruthenium on the structure and catalytic performance of mesoporous silica (smaller and larger pore) supported cobalt Fischer–Tropsch catalysts

Jingping Hong [a,b], Petr A. Chernavskii [c], Andrei Y. Khodakov [a,*], Wei Chu [b,*]

[a] Unité de Catalyse et de Chimie du Solide - UMR 8181 CNRS, USTL-ENSCL-ECLille, Bât. C3, Cité scientifique, 59655 Villeneuve d'Ascq, France
[b] Lab 230, Department of Chemical Engineering, Sichuan University, Chengdu 610065, Sichuan, China
[c] Department of Chemistry, Moscow State University, 119992 Moscow, Russia

ARTICLE INFO

Article history:
Available online 22 November 2008

Keywords:
Fischer–Tropsch synthesis
Cobalt catalysts
Texture
Ruthenium
Mesoporous silicas

ABSTRACT

The effects of promotion with ruthenium on the structure of cobalt catalysts and their performance in Fischer–Tropsch synthesis were studied using MCM-41 and SBA-15 as catalytic supports. The catalysts were characterized by N_2 physisorption, H_2-temperature programmed reduction, in situ magnetic measurements, X-ray diffraction and X-ray photoelectron spectroscopy. It was found that monometallic cobalt catalysts supported by smaller pore mesoporous silicas (d_p = 3–4 nm) had much lower activity in Fischer–Tropsch synthesis than their larger pore counterparts (d_p = 5–6 nm). Promotion with ruthenium of smaller pore cobalt catalysts led to a considerable increase in Fischer–Tropsch reaction rate, while the effect of the promotion with ruthenium was less significant with the catalysts supported by larger pore silicas.

Characterizations of smaller pore cobalt catalysts revealed strong impact of ruthenium promotion on the repartition of cobalt between reducible Co_3O_4 phase and barely reducible amorphous cobalt silicate in the calcined catalyst precursors. Smaller pore monometallic cobalt catalysts showed high fraction of barely reducible cobalt silicate. Promotion with ruthenium led to a significant increase in the fraction of reducible Co_3O_4 and in decrease in the amount of cobalt silicate. In both calcined monometallic and Ru-promoted cobalt catalysts supported by larger pore silicas, easy reducible Co_3O_4 was the dominant phase. Promotion with ruthenium of larger pore catalysts had smaller influence on cobalt dispersion, fraction of reducible cobalt phases and thus on catalytic performance.

1. Introduction

Fischer–Tropsch (FT) synthesis converts coal-, biomass- and natural gas-derived syngas into super clean diesel fuels with high cetane numbers, low contents of sulfur and aromatics [1–3]. It has gained recently renewed interest because of high crude oil prices and new environmental requirements for the residual sulfur (30–50 ppm) in diesel fuel.

FT synthesis is a reaction which proceeds on supported metal catalysts. Cobalt-based catalysts are preferred for the synthesis of high molecular weight paraffins [1–3], as they own high activity, high selectivity to linear hydrocarbons, low activities for the water-gas shift reaction, and lower price compared to those of noble metals. Since the catalytically active phase of this reaction is metallic cobalt, the behavior of cobalt catalysts in FT synthesis strongly depends on the dispersion and reducibility of cobalt species. Design of efficient cobalt catalysts with high concentration of cobalt metal sites, high FT catalytic activity and high selectivity to desired products still remains a challenge.

Hence, high surface area ordered mesoporous materials (such as MCM-41 and SBA-15) and different promoters (such as ruthenium, zirconium, lanthanum, rhodium, boron, platinum) have been explored recently. MCM-41 and SBA-15 mesoporous materials as supports for cobalt FT catalysts have been addressed in several publications [4–11]. Our previous reports [12–15] have shown that cobalt dispersion in ordered mesoporous silicas is principally affected by pore diameters; smaller cobalt particles are usually observed in smaller pore silicas. It appears [13] that catalyst texture may even have a more significant impact on cobalt dispersion than overall cobalt loading. The sizes of cobalt particles could be controlled by pore diameters even at high cobalt contents. Due to the strong interaction of cobalt species and supports in these catalysts, the reducibility of small cobalt particles in small

* Corresponding authors.
E-mail addresses: Andrei.khodakov@univ-lille1.fr (A.Y. Khodakov), Chuwei65@yahoo.com.cn (W. Chu).

0920-5861/$ – see front matter © 2008 Elsevier B.V. All rights reserved.
doi:10.1016/j.cattod.2008.10.009

pore was relatively low, which led to poor FT synthesis performance.

Analysis of recent literature data [3a, 3b] suggests that the introduction of noble metals could result in several phenomena: much easier reduction of cobalt oxide particles, formation of bimetallic particles and alloys, a lower fraction of barely reducible mixed oxides, enhancement in cobalt dispersion, inhibition of catalyst deactivation, appearance of additional sites of hydrogen activation, and increase in the intrinsic reactivity of surface sites.

This work focuses on the effects of ruthenium addition on the structures and cobalt species in mesoporous-silica supported cobalt catalysts, and their catalytic performances in FT synthesis. Nitrogen adsorption, X-ray diffraction (XRD), Temperature Programmed Reduction (TPR), in situ magnetic measurements and X-ray photoelectron spectroscopy (XPS) were applied to characterize the catalysts. The catalytic performances of mesoporous silica supported cobalt catalysts were evaluated in a fixed bed micro-reactor.

2. Experimental

2.1. Catalyst preparation

2.1.1. Support preparation

The synthesis of Si1 sample (MCM41 type) was carried out according to the procedure reported in Ref. [12]. This material was prepared by stirring 37.50 g of 25% solution of cetyltrimethyl ammonium chloride (CTMACl) and 1.79 g of 28% NH_4OH solution, 9.46 g tetramethylammonium hydroxide pentahydrate (TMAOH), 10 g of fumed silica and 20.36 g of deionized water. The reacting mixture was stirring for 30 min and then transferred into a hermetically closed polypropylene flask and heating in an oven at 80 °C for 48 h. The resulting gel was washed thoroughly with distilled water, dried at 80 °C for 12 h and calcined first in flowing nitrogen for 5 h at 500 °C, then in flowing air at 550 °C for 5 h.

The preparation of Si 2 sample (SBA15 type) was performed in a similar manner as described in Ref. [16]. To get 10 g support, 16.32 g of P123 (poly (ethylene glycol)–poly (propylene glycol)–poly (ethylene glycol)) was dissolved in a mixture of 514.39 g water and 97.61 g 2 mol/L HCl under stirring. As a silica source, 34.68 g tetraethylortho-silicate (TEOS) was the last component added to the synthesis mixture. The above mixture was kept at 40 °C under stirring for 24 h. The final molar ratio was 1 TEOS:1.16 HCl:206.06 H_2O:0.017 P123. Then using the same procedure as in the preparation of Si1, the mixture was transferred to a hermetically closed polypropylene flask and heated in an oven at 80 °C for 48 h. The as-prepared Si2 was separated by filtration, washed thoroughly by distilled water, dried at 80 °C for 12 h, and calcined first in flowing nitrogen at 500 °C for 5 h, then in flowing air for another 5 h at 550 °C.

The procedure of Si3 (SBA-15 type) synthesis was similar to that of Si2. Concentration of HCl was however 10 mol/L instead of 2 mol/L in the synthesis of Si2. The final molar ration of materials was 1 TEOS:5.58 HCl:197.34 H_2O:0.017 P123.

2.1.2. Cobalt deposition

In preparation of monometallic catalysts, cobalt was introduced to silicas by aqueous incipient wetness impregnation (IWI) using solutions containing the desired amount of cobalt nitrate. Ruthenium nitrosyl nitrate was added to the impregnation solution in preparation of Ru-promoted cobalt catalysts. The samples were dried overnight at ambient temperature and then calcined in the flow of dry air at 250 °C for 5 h. Before reaction, all the catalysts were reduced in the flow of hydrogen at 400 °C for 5 h. The chemical composition of catalysts is presented in Table 1.

Table 1
Chemical composition of catalysts.

Supports	Type	Catalysts	Cobalt content (wt.%)	Ruthenium content (wt.%)
Si1	MCM-41	CoSi1	10	0
		CoRuSi1	10	0.3
Si2	SBA-15-1	CoSi2	10	0
		CoRuSi2	10	0.3
Si3	SBA-15-2	CoSi3	10	0
		CoRuSi3	10	0.3

2.2. Catalyst characterization

2.2.1. Surface area and pore size distribution

The BET surface area, pore volume, average pore diameter and pore size distribution of the catalysts were determined by N_2 physisorption at 77 K using a Micromeritics ASAP 2010 apparatus. Prior to the experiments, the samples were outgassed at 150 °C for 5 h. The total pore volume (TPV) was calculated from the amount of vapor adsorbed at a relative pressure (P/P_0) close to unity assuming that the pores are filled with the condensate in liquid state, where P and P_0 are the measured and equilibrium pressures, respectively. The pore size distribution curves were calculated from the desorption branches of the isotherms using BJH formula [17].

2.2.2. X-ray diffraction measurements

XRD patterns were recorded at room temperature by a Siemens D5000 diffractometer using Cu Kα radiation using the Co_3O_4 (4 4 0) diffraction peak at $2\theta = 65.34$. The average size of Co_3O_4 particle was calculated according to the Sherrer equation [18].

$$d = \frac{0.89\lambda}{B\cos\theta} \times \frac{180^\circ}{\pi}$$

where d is the average crystallite diameter, λ is the peak length, and B is the full width half in degrees.

2.2.3. X-photoelectron spectroscopy

XPS spectra of calcined catalysts were recorded using VG ESCALAB 220XL spectrometer equipped with a 300 W Al Kα source ($h\upsilon$ = 1486.6 eV) operated at 15 kV and 16 mA. The binding energy of Si 2p (103.8 eV) from silica support was used as a reference. The measurements were performed in high vacuum level ($\sim 10^{-8}$ Torr) at room temperature. The powdered catalyst was pressed as a thin pellet onto an indium block. The experimental Co 2p XPS spectra of the catalysts were normalized by the intensity of Si 2p line. The particle sizes of Co_3O_4 particles were estimated with the Kerkhof–Moulijn formula [19], the calculation details are also available from Ref. [12].

The size values of Co_3O_4 particles in the catalysts were utilized to calculate the corresponding cobalt metal particle size according to the relative molar volumes of metallic cobalt and Co_3O_4. The resulting conversion factor for the diameter of a given Co_3O_4 particle being reduced to metallic cobalt is: $d(Co^0) = 0.75\ d(Co_3O_4)$ [20,21]. Cobalt dispersion (D, %) was calculated from the average metal particle sizes (nm) assuming spherical uniform particles with site density 14.6 atoms/nm^2, by the use of formula: $D = 96/d$ [20,21].

2.2.4. H_2-temperature programmed reduction

The temperature-programmed reduction profiles were obtained by passing 5% H_2/Ar gas mixture through the catalyst while increasing the temperature at a linear rate. The experiments were carried out in the reactor. The amount of samples for all experiments was about 50 mg. The gas flow velocity was 30 ml/min, and the rate of temperature ramping was 3 °C/min.

2.2.5. In situ magnetic measurements

In situ magnetic measurements were performed using a Foner vibrating-sample magnetometer as described previously [22]. Design of magnetometer allows recording curves of magnetization during temperature-programmed heating or under isothermal conditions at 5–700 °C. The magnetometer is fitted with a continuous-flow quartz microreactor equipped with a built-in Pt–PtRh thermocouple. The experiments were conducted by passing pure H_2 through the catalyst while increasing the temperature at a linear rate. The amount of samples for all measurements was around 20 mg. The rate of temperature ramping was 28.2 °C/min, and the temperature measure range was from 20 to 400 °C, then keeping it isothermal at 400 °C. The appearance of metallic cobalt species in the samples was monitored in situ by a continuous increase in sample magnetization during the reduction.

2.3. Catalytic measurements

The Fischer–Tropsch reaction was carried out in a fixed-bed stainless-steel tubular microreactor (d_{int} = 9 mm) operating at 190 °C under atmospheric pressure with a H_2/CO molar ratio of 2. The thermocouple was in direct contact with the catalyst. The catalyst was crushed and sieved to obtain catalyst grains 63–200 μm in diameter. The catalyst loading was typically 0.5 g. Before reaction, the samples were reduced in hydrogen flow at 400 °C for 5 h. The carbon monoxide contained 5% nitrogen, which was used as an internal standard for calculating carbon monoxide conversion. The reactor and gas transfer lines were placed in an oven and constantly heated at 160 °C, in order to avoid possible condensation of the reaction products. The reaction products were analyzed on-line by gas chromatography. Analysis of H_2, CO, CO_2, and CH_4 was performed by a 13X molecular sieve column and a thermal conductivity detector. Hydrocarbons (C1–C18) were analyzed by a flame-ionization detector with a 10% CP-Sil5 on Chromo Sorb WHP column. The hydrocarbon selectivities were calculated on carbon basis. The Anderson–Schulz–Flory (ASF) chain growth probabilities were calculated from the slope of the curve ln(Sn/n) versus n, where n is the carbon number and Sn is the selectivity to the Cn hydrocarbon. The chain growth probability was calculated for the C4–C16 hydrocarbon range. The FT reaction rate is expressed as cobalt-time yield (in moles of converted CO per second divided by the total amount of cobalt (in moles) loaded into the reactor).

3. Results and discussion

3.1. Catalyst porosity

The nitrogen adsorption–desorption isotherms for both Si1, Si2 and Si3 silicas and cobalt monometallic and Ru-promoted catalysts are shown in Fig. 1a–c. The original Si1 silica (Fig. 1a) presents a type IV isotherm according to the classification of Brunauer et al. [23]. The isotherm displays the typical step at $P/P_0 \sim 0.3$ characteristic of capillary condensation within narrow mesopores of the MCM-41 structure. Calculations using BJH method show that the S1 silica has a narrow pore size distribution with an average pore diameter of 3.4 nm. Modification of Si1 silica either with cobalt or with both cobalt and ruthenium results in a considerable modification of the shape of nitrogen adsorption-desorption isotherms. In the isotherms of the cobalt catalysts, the step at P/P_0 = 0.3 characteristic of the MCM-41 mesoporous structures disappears. This observation is consistent with previous report [6] about the effect of impregnation with cobalt nitrate solutions on the structure of MCM-41 materials. Table 1 shows that the modification with cobalt also leads to a dramatic decrease in the BET surface area and total pore volume. In cobalt and cobalt–ruthenium catalysts supported by Si1 silica BJH

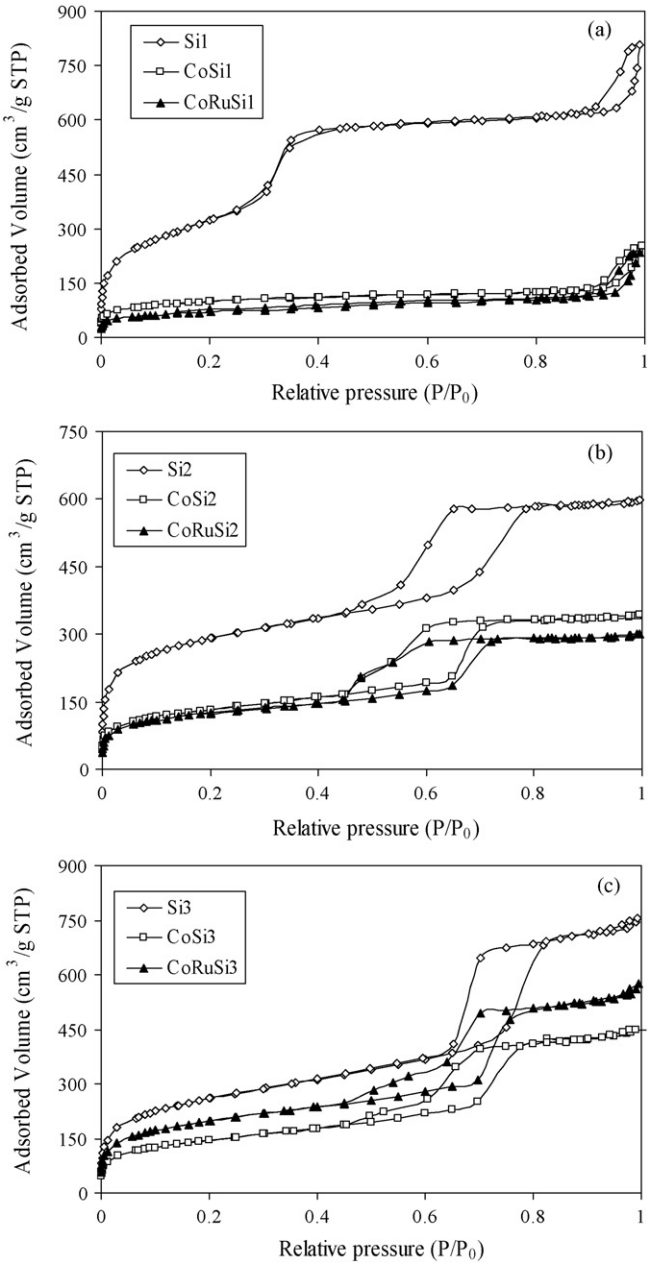

Fig. 1. Nitrogen adsorption–desorption isotherms measured for silica supports and cobalt catalysts: (a) Si1 supported catalysts; (b) Si2 supported catalysts; (c) Si3 supported catalysts.

analysis (Fig. 1a) indicates the simultaneous presence of both micropores (d_p < 2 nm) and a small population of relatively larger mesopores (d_p = 30 nm).

S2 and S3 silicas exhibit irreversible type IV isotherms with a H1 hysteresis loop (Fig. 1b and c) which are typical of SBA-15 type materials with cylindrical pores. The P/P_0 position of the inflection point is a function of the pore diameter. The pore diameter of the original S2 and S3 silicas calculated using the BJH method are respectively 4.4 and 5.7 nm. Broader hysteresis loop observed after modification either with cobalt or with cobalt and ruthenium suggests broadening pore size distribution curves in the FT catalysts supported on Si2 and Si3 silicas.

Information about the texture of the supports and catalysts is presented in Table 2. The BET surface area in all periodic mesoporous silicas (Si1, Si2, Si3) was higher than 900 m^2/g. The

Table 2
Adsorption properties of supports and cobalt based catalysts.

Supports	S_{BET} (m^2/g)	TPV (cm^3/g)	Pore diameter (nm)	Catalysts	S_{BET} (m^2/g)	TPV (cm^3/g)	Pore diameter (nm)
Si1	1180	1.05	3.4	CoSi1	349	0.30	Bimodal PSD[a]
				CoRuSi1	439	0.31	
Si2	1029	0.92	4.4	CoSi2	471	0.56	4.5
				CoRuSi2	441	0.50	4.4
Si3	935	1.13	5.7	CoSi3	534	0.67	6.1
				CoRuSi3	519	0.69	6.1

[a] Bimodal pore size distribution (PSD), simultaneous presence of micropores ($d_p < 2$ nm) and large mesopores ($d_p = 30$ nm).

total pore volumes of the supports were varied from 0.90 to 1.20 cm^3/g. After impregnation, both BET surface area and total pore volume significantly decreased. The drop of surface area can be due both to plugging silica pores with cobalt oxide crystallites and to the effect of the silica "dilution" because of the presence of cobalt species. The magnitude of surface area drop suggests, however, that pore plugging contributes more significantly to the surface area decrease than silica "dilution".

In this paper, the catalysts supported by Si1 and Si2 silicas with pore diameters of 3.3 nm and 4.4 nm respectively, are considered as small pore catalysts, while their counterparts supported by Si3 silica are seen as larger pore catalysts.

3.2. Cobalt species and particle sizes

The XRD patterns of Co and CoRu catalysts are presented in Fig. 2. XRD patterns characteristic of Co_3O_4 were detected for all calcined catalysts. The Co_3O_4 crystallite sizes (Table 3) were calculated from the widths of XRD peaks using the Sherrer equation ($2\theta = 65.344$). The Co_3O_4 crystallite diameter varied only very slightly as a function of silica pore size. After the introduction of ruthenium, the intensity of XRD peaks of Co_3O_4 crystallites was considerably enhanced in Si2 supported catalyst, the size of Co_3O_4 crystallites did not change significantly. The diameter of Co_3O_4 crystallites in Si1 supported cobalt catalyst decreased to some extent after the addition of ruthenium, while CoSi3 and CoRuSi3 showed similar Co_3O_4 particle size (Table 3). Some decrease in Co_3O_4 crystallite size after promotion of silica supported catalysts with noble metals (Ru, Re, Pt) was also observed in previous reports [24,25]. Our earlier work [24] suggests that this decrease could be related to a higher concentration of cobalt oxide crystallization sites in the presence of noble metals during decomposition of cobalt nitrate complexes. Higher concentration of crystallization sites at the similar cobalt content would result in larger number of cobalt particles and consequently higher cobalt dispersion in the catalysts.

Fig. 3 illustrates the Co 2p spectra obtained from mesoporous silica supported cobalt catalysts and their ruthenium promoted counterparts after calcination at 250 °C for 5 h. For smaller pore catalysts (CoSi1 and CoSi2), the binding energies of Co $2p_{3/2}$ were 781.9 and 781.7 eV, respectively, and a high intensity of the shake-up satellite peaks was observed. These features indicate the presence of Co^{2+} species in amorphous cobalt silicate [12,26] and could be taken as evidence of a strong interaction of the cobalt species with the surface of support. After the addition of ruthenium, the binding energies of Co $2p_{3/2}$ were shifted towards lower energies, from 781.9 to 780.6 eV and from 781.7 to 780.0 eV

Table 3
XRD and XPS analysis of the catalysts.

Catalyst	XPS atomic ratio (%)			Co_3O_4 crystallite diameter (nm)		Estimated cobalt dispersion (%, XPS)
	Co 2p	O 1s	Si 2p	XRD	XPS	
CoSi1	1.80	61.80	31.94	8.7	–	–
CoRuSi1	2.93	58.71	29.53	6.4	2.1	47.4
CoSi2	2.06	60.83	31.59	9.2	–	–
CoRuSi2	4.80	55.75	27.82	8.8	Very small	Highly dispersed
CoSi3	1.34	60.50	32.72	9.8	7.2	17.8
CoRuSi3	1.11	61.37	32.28	9.2	8.7	14.7

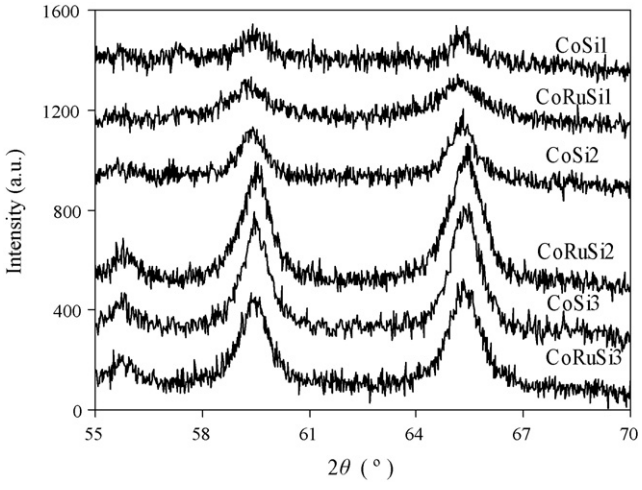

Fig. 2. XRD diffraction patterns of silica supported Co and CoRu catalysts.

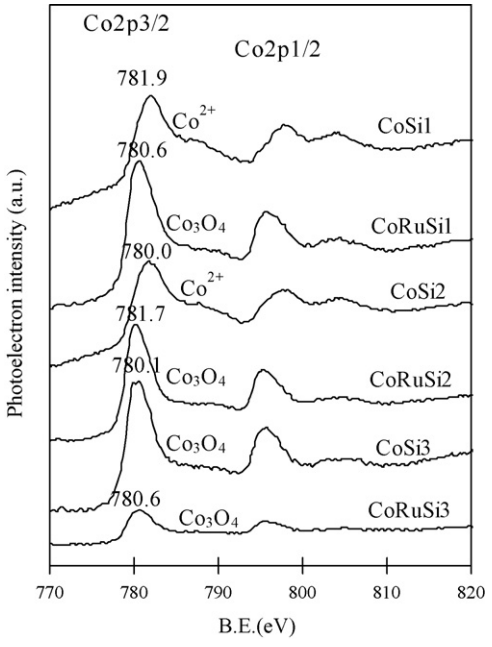

Fig. 3. XPS spectra of the Co 2p level for silica supported Co and CoRu catalysts.

for Si1 and Si2, respectively, and showed a low intensity of the shake-up satellite peaks, which was typical for Co^{2+}/Co^{3+} ions in the Co_3O_4 spinel phase [27]. Therefore, Co_3O_4 was the dominant Co phase in calcined CoRuSi1 and CoRuSi2 catalysts, while in calcined CoSi1 and CoSi2 catalysts the fraction of cobalt silicate was much higher. In the case of CoSi3 catalysts, the binding energy of Co $2p_{3/2}$ was slightly shifted towards higher energies (from 780.1 to 780.6 eV), and the intensity of XPS signal decreased in the promoted catalyst, however, the shapes of the Co 2p spectra remain similar, Co_3O_4 is the dominant cobalt phase in both CoSi3 and CoRuSi3 samples. The intensities of XPS peaks for Ru were below the detection limit, because of the relatively small amount of ruthenium in the catalysts (0.3 wt.%).

XPS is a technique which is selectively sensitive to the surface composition of the catalysts grains (depth of analysis ≈6 nm). In the bulk cobalt oxide clusters, only a part of cobalt atoms is detectable by XPS. The I_{Co}/I_{Si} ratio obtained from the intensity of XPS line provides valuable information about the sizes of Co clusters. For these catalysts I_{Co}/I_{Si} ratio equal to 3.09 corresponds to monolayer coverage. More information about calculating particle sizes from XPS data is available in the paper by Kerkhof and Moulijn [19] and in our earlier report [12]. The sizes of Co_3O_4 particles obtained from the intensity of XPS and the Kerkhof–Moulijn method are displayed in Table 3. Note that cobalt oxide particle size calculations from XPS data were only performed only for catalysts where Co_3O_4 was the dominant phase. The Co/Si ratio for CoRuSi2 catalyst was higher than it can be expected from the monolayer coverage. This is indicative of high cobalt dispersion in this catalyst. Table 3 also provided the elemental composition on the surface of Co and CoRu catalysts measured by XPS. The cobalt surface atom ratio of CoSi1 and CoSi2 samples increased by the introduction of a small amount ruthenium. In agreement with XRD data, these results indicated that the addition of 0.3% Ru in small pore silica supported cobalt catalysts could both change repartition of cobalt phase between Co_3O_4 and cobalt silicate and enhance the cobalt dispersion.

3.3. Cobalt reducibility

The influences of supports on the reducibility of the supported cobalt catalysts were studied by temperature programmed reduction (TPR). The TPR profiles of both monometallic and Ru-promoted Co/SiO_2 catalysts, shown in Fig. 4, exhibited several peaks. The occurrence of multiple reduction peaks indicated the presence of several reducible cobalt oxide species. Caused by the low calcination temperature, some low temperature TPR peaks might also be assigned to the decomposition of residual cobalt nitrate [28]. The TPR peaks in the temperature range of 150–450 °C also comprised the two step reduction of Co_3O_4 ($Co_3O_4 \rightarrow CoO \rightarrow Co^0$) [29–33]. The broad peak which located higher than 450 °C was assigned to the reduction of those cobalt oxide species (Co^{2+} and Co^{3+}), which were in interaction with the support. Note that presence of low temperature peaks in TPR profiles of monometallic catalysts precalcined at low temperature does not indicate much easier reducibility of these catalysts. The TPR profiles of cobalt–ruthenium based catalysts were much different from that of the catalyst without ruthenium addition, which indicated that cobalt reducibility was significantly changed by the addition of ruthenium.

The complexity of hydrogen consumption profiles in TPR experiments made it difficult to identify the exact nature of reduction stages of these catalysts. It is known that the magnetic method is selectively sensitive to the concentration of metallic cobalt phase. Thus, it appears to be helpful for interpreting the complex TPR profiles. Our previous report showed [22] that hydrogen partial pressure had strong effect on the catalyst magnetization. This suggests that in pure hydrogen cobalt species can be reduced at lower temperatures than in H_2/Ar mixtures. Thus, TPR peaks temperatures of metallic cobalt generation, measured in 5% H_2/Ar, were higher than those in the relevant measurements of magnetization in pure hydrogen.

The effects of ruthenium addition on the properties of metallic cobalt generations of these cobalt samples could be seen from Fig. 5. Metallic cobalt was the only ferromagnetic phase presented in the catalysts during the reduction. Since magnetic method was selectively sensitive to the presence of ferromagnetism, the total amount of metallic cobalt could be evaluated from magnetization measurements. The presence of ruthenium resulted in a decrease in the temperature of appearance of the metallic cobalt phase. Meanwhile, the intensity of magnetization which corresponds to the concentration of metallic cobalt phase was significantly enhanced by the introduction of ruthenium in smaller pore silicas (Si1 and Si2) supported cobalt catalysts. Compared the concentration of metallic cobalt phase in these investigated samples, after reduction in pure hydrogen at 400 °C, from Fig. 5, they followed this order: $CoSi_3 \approx CoRuSi_3 > CoRuSi_1 \approx CoSi_2$.

3.4. Catalytic behavior

The catalytic activities of Co based and CoRu based catalysts were measured in a fixed-bed reactor at 190 °C, 1 bar, $H_2/CO = 2$ and GHSV = 1800 ml/(g_{cat} h). Carbon dioxide was not observed in

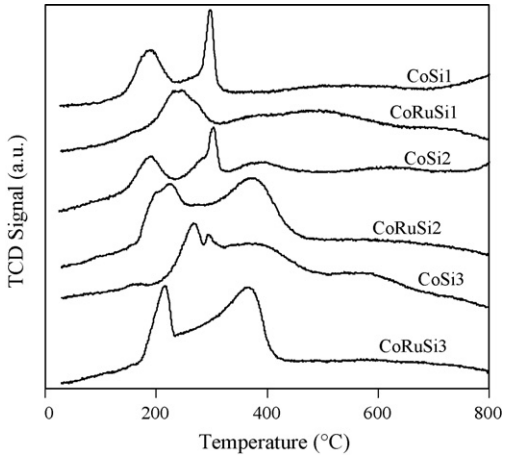

Fig. 4. TPR patterns of silica supported Co and CoRu catalysts.

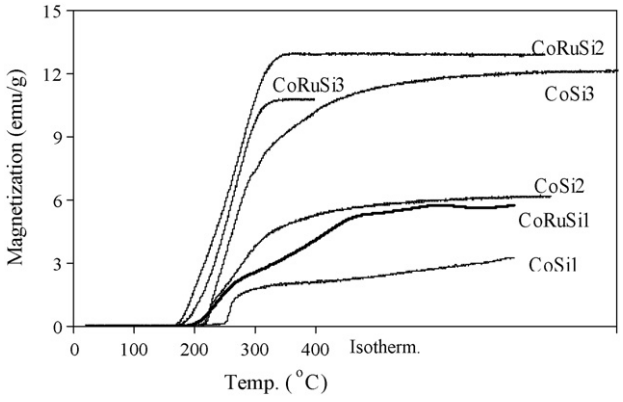

Fig. 5. In situ magnetization of silica supported Co and CoRu catalysts during the reduction in pure hydrogen.

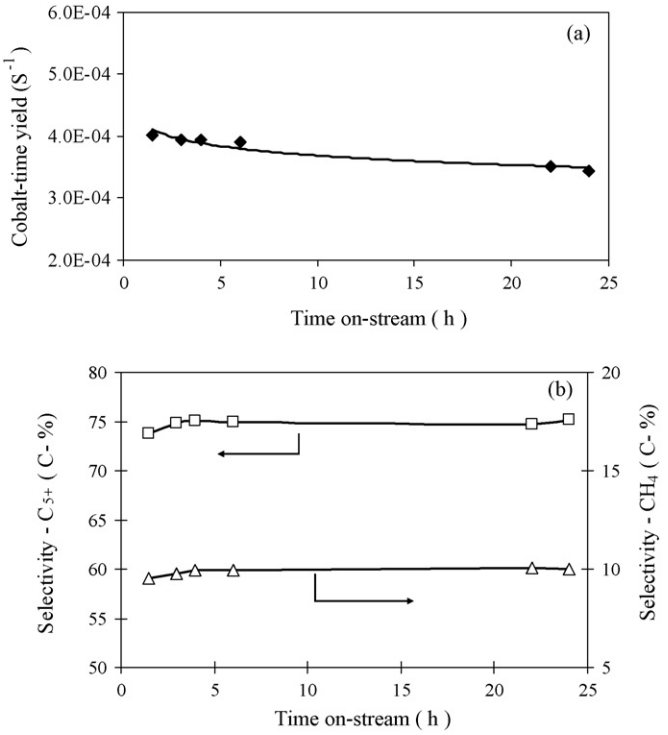

Fig. 6. FT reaction rates (a), methane, and C_{5+} selectivities (b) as functions of time on stream on CoSi3 sample (T = 190 °C, H_2/CO = 2, P = 1 atm, GHSV = 1800 ml/(g h)).

the reaction process at above conditions. The activity and selectivity values reported here correspond to those at the period of quasi-steady behavior. The FT reaction rates (cobalt time yields) were calculated from the FT reaction rates from carbon monoxide conversions and gas hourly space velocities, then the rates were normalized by the number of cobalt atoms loaded in the reactor.

Fig. 6 showed the performances of FT reaction rate, methane selectivity and C_{5+} selectivity; versus the time on stream for CoSi3 sample. FT reaction rates decreased slightly and gradually with increasing time on stream during 24 h test; and the quasi-steady state was attained after about 4 h, whereas the selectivities of hydrocarbons almost unchanged. The reaction rates were calculated from CO space velocity and its conversion at 24 h on stream.

The experimental results were shown in Table 4 and Fig. 7. The catalytic performances of CoSi1 and CoSi2 samples were remarkably enhanced by the Ru addition and promotion, the CO conversion increased from 1.0% to 4.72% for Si1 supported cobalt catalyst, and from 3.3% to 8.9% for Si2 supported cobalt catalyst, respectively. While the activity of the Si3 supported cobalt catalyst decreased slightly with Ru addition. XRD data (Fig. 2, Table 3)

Table 4
The effect of Ru addition on the catalytic performance of Co supported catalysts.

Catalyst	Conversion CO (%)	Cobalt time yield (10^{-4} s^{-1})	Selectivities CH_4 (%)	Selectivities C_{5+} (%)	α[a]
CoSi1	1.0	0.4	21.9	45.7	0.58
CoRuSi1	4.7	2.0	11.9	60.0	0.74
CoSi2	3.3	1.4	9.8	76.0	0.80
CoRuSi2	8.9	3.8	10.1	73.2	0.79
CoSi3	9.3	3.9	9.9	75.1	0.80
CoRuSi3	7.8	3.3	9.3	76.3	0.81

T = 190 °C, H_2/CO = 2, P = 1 atm, GHSV = 1800 ml/(g h).
[a] ASF chain growth probability.

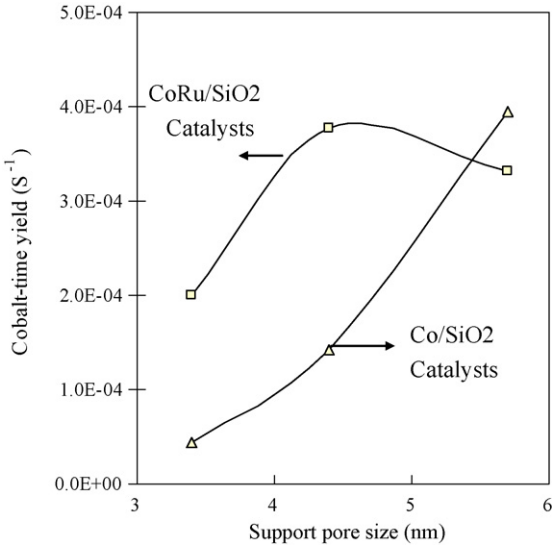

Fig. 7. Relation between cobalt-time yield and pore size of support.

demonstrated that cobalt dispersion did not significantly change after promotion with Ru. XPS suggests (Fig. 3) the addition of ruthenium contributed to the formation of Co_3O_4 phase instead of cobalt silicate. Cobalt silicate has much lower reducibility in hydrogen than Co_3O_4 crystalline phase and does not produce active sites for FT synthesis. CoSi1 and CoSi2 catalysts which contained high fractions of cobalt silicate showed much lower cobalt-time yield (Fig. 7) than the ruthenium-promoted counterparts. As for CoSi3 and CoRuSi3, the dominant Co phase in both calcined samples is Co_3O_4. XRD, XPS, TPR and magnetic measurements indicate similar dispersion and reducibility for these catalysts. Thus, the effect of promotion with Ru on the cobalt time-yield (Fig. 7) was less significant than that with larger pore catalysts. Hence, the effect of ruthenium promotion on catalytic performance of CoSi3 was less pronounced.

It can be suggested that for small pore catalysts, the addition of ruthenium not only improved the reducibility of cobalt compounds into Co^0 but also significantly increased the concentration of active sites and improved catalytic performance in FT synthesis.

The catalytic and characterization results emphasize the role of Ru promoter on the fraction of Co_3O_4 phase in smaller and larger pore cobalt FT catalysts. It is shown that formation of easy reducible Co_3O_4 is considerably enhanced in smaller pore catalysts in the presence of ruthenium. It seems that ruthenium affects crystallization of Co_3O_4 particles in silica small pores. Higher fraction of Co_3O_4 crystalline phase in Ru-promoted cobalt silica supported catalysts with smaller pores improves cobalt reducibility and leads to better catalytic performance in FT synthesis. The uncovered effect of catalyst pore sizes on the fraction of Co_3O_4 reducible phase and amorphous cobalt silicate cannot be assigned to the different surface area of the supports. Indeed, all the supports and all the catalysts have comparable BET surface areas (Table 2, 935–1180 m^2/g for the supports and 349–519 m^2/g for cobalt catalysts).

4. Conclusions

The results show strong impact of catalyst pore sizes and ruthenium promotion on the repartition of cobalt between Co_3O_4 and amorphous cobalt silicate species in calcined catalyst precursors, cobalt dispersion and on the overall FT catalytic

performance. Higher fraction of Co_3O_4 was found in larger pore silicas and in smaller pore silicas promoted with ruthenium. Lower concentration of amorphous hardly reducible cobalt silicate and enhanced cobalt reducibility are likely to be the reasons responsible of higher FT reaction rates and high C_{5+} selectivity over small pore (3.4–4.4 nm) cobalt–ruthenium bimetallic catalysts. The effect of promotion with Ru on cobalt repartition between Co_3O_4 and cobalt silicate and FT catalytic performance was less significant on larger pore silica.

Acknowledgements

Jingping Hong thanks the PhD scholarship support of the Embassy of France in China. The supports from the Natural Science Foundation of China (NSFC 205903603) and the 985 Project and 211 Project of Sichuan University are also acknowledged. P.A.C. acknowledges the financial support of the Russian Foundation for Fundamental Research (grant #06-03-32500-a). The authors thank L. Burylo, M. Frère, O. Gardoll for helps with X-ray diffraction, XPS, TPR. The authors would like to thank Prof. E. Payen, Prof. X.Y. Dai, the colleagues in the Unité de catalyse et de chimie du solide, UMR CNRS 8181 of France and those of 230 Lab of Sichuan University for useful discussions.

References

[1] M.E. Dry, Catal. Today 71 (2002) 227.
[2] E. Iglesia, Appl. Catal. A 161 (1997) 59.
[3] (a) A.Y. Khodakov, W. Chu, P. Fongarland, Chem. Rev. 107 (2007) 1692;
(b) W. Chu, P.A. Chernavskii, L. Gengembre, G.A. Pankina, P. Fongarland, A.Y. Khodakov, J. Catal. 252 (2007) 215;
(c) W. Chu, L.N. Wang, P.A. Chernavskii, A. Khodakov, Angew. Chem. Int. Ed 47 (2008) 5052.
[4] H. Li, S. Wang, F. Ling, J. Li, J. Mol. Catal. A 244 (2006) 33.
[5] J. Panpranot, S. Kaewgun, P. Praserthdam, React. Kinet. Catal. Lett. 85 (2005) 299.
[6] A.Y. Khodakov, V.L. Zholobenko, R. Bechara, D. Durand, Microporous Mesoporous Mater. 79 (2005) 29.
[7] M. Wei, K. Okabe, H. Arakawa, Y. Teraoka, New J. Chem. 27 (2003) 928.
[8] J. Panpranot, J.G. Goodwin Jr., A. Sayari, Catal. Today 77 (2002) 269.
[9] M. Wei, K. Okabe, H. Arakawa, Y. Teraoka, React. Kinet. Catal. Lett. 77 (2002) 381.
[10] J. Panpranot, J.G. Goodwin Jr., A. Sayari, J. Catal. 211 (2002) 530.
[11] D. Yin, W. Li, W. Yang, H. Xiang, Y. Sun, B. Zhong, S. Peng, Microporous Mesoporous Mater. 47 (2001) 15.
[12] A.Y. Khodakov, A. Griboval-Constant, R. Bechara, V.L. Zholobenko, J. Catal. 206 (2002) 230.
[13] A.Y. Khodakov, R. Bechara, A. Griboval-Constant, Appl. Catal. A 254 (2003) 273.
[14] A.Y. Khodakov, J.-S. Girardon, A. Griboval-Constant, A.S. Lermontov, P.A. Chernavskii, Stud. Surf. Sci. Catal. 147 (2004) 295.
[15] A.Y. Khodakov, R. Bechara, A. Griboval-Constant, Stud. Surf. Sci. Catal. 142 (2002) 1133.
[16] A.Y. Khodakov, V.L. Zholobenko, M. Imeror-Clerc, D. Durand, J. Phys. Chem. B 109 (2005) 22780.
[17] E.P. Barrett, L.G. Joyner, P.P. Halenda, J. Am. Chem. Soc. 73 (1951) 373.
[18] B.D. Cullity, Elements of X-ray Diffraction, Addision-Wesley, London, 1978.
[19] F.P.J. Kerkhof, J.A. Moulijn, J. Phys. Chem. 83 (1979) 1612.
[20] S. Sun, N. Tsubaki, K. Fujimoto, Appl. Catal. A 202 (2000) 121.
[21] D. Schanke, S. Vada, E.A. Blekkan, A.M. Hilmen, A. Hoff, A. Holmen, J. Catal. 156 (1995) 56.
[22] P.A. Chernavskii, A.Y. Khodakov, G.V. Pankina, J.-S. Girardon, E. Quinet, Appl. Catal. A 306 (2006) 108.
[23] S. Brunauer, L.S. Deming, W.S. Deming, E. Teller, J. Am. Chem. Soc. 62 (1940) 1723.
[24] J.-S. Girardon, E. Quinet, A. Griboval-Constant, P.A. Chernavskii, L. Gengembre, A.Y. Khodakov, J. Catal. 248 (2007) 143.
[25] D. Schanke, S. Vada, E.A. Blekkan, A.M. Hilmen, A. Hoff, A. Holmen, J. Catal. 156 (1995) 85.
[26] S.W. Ho, M. Horialla, D.M. Hercules, J. Phys. Chem. 94 (1990) 6396.
[27] Y. Brik, M. Kacimi, M. Ziyad, F. Bozon-Verduraz, J. Catal. 202 (2001) 118.
[28] O. Borg, E.A. Blekkan, S. Eri, D. Akporiaye, B. Vigerust, E. Rytter, A. Holmen, Top. Catal. 45 (2007) 39.
[29] R. Bechara, D. Balloy, J.-Y. Dauphinand, J. Grimblot, Chem. Mater. 11 (1999) 1703.
[30] D.G. Castner, P.R. Watson, I.Y. Chan, J. Phys. Chem. 94 (1990) 819.
[31] A.Y. Khodakov, J. Lynch, D. Bazin, B. Rebours, N. Zanier, B. Moisson, P. Chaumette, J. Catal. 168 (1997) 16.
[32] B. Ernst, A. Bensaddik, L. Hilaire, P. Chaumette, A. Kiennemann, Catal. Today 39 (1998) 329.
[33] A.Y. Khodakov, A. Griboval-Constant, R. Bechara, F. Villain, J. Phys. Chem. B 105 (2001) 9805.